Symmetry breaking and phase coexistence in a driven diffusive two-channel system

Vladislav Popkov[1,2] and Ingo Peschel[1]
[1]*Fachbereich Physik, Freie Universität Berlin, Arnimallee 14, D-14195 Berlin, Germany*
[2]*Institute for Low Temperature Physics, 310164 Kharkov, Ukraine*
(Received 26 September 2000; revised manuscript received 6 April 2001; published 26 July 2001)

We consider classical hard-core particles moving on two parallel chains in the same direction. An interaction between the channels is included via the hopping rates. For a ring, the stationary state has a product form. For the case of coupling to two reservoirs, it is investigated analytically and numerically. In addition to the known one-channel phases, two new regions are found, in particular one, where the total density is fixed, but the filling of the individual chains changes back and forth, with a preference for strongly different densities. The corresponding probability distribution is determined and shown to have a universal form. The phase diagram and general aspects of the problem are discussed.

DOI: 10.1103/PhysRevE.64.026126 PACS number(s): 05.70.Ln, 64.60.Cn, 02.50.Ga, 05.70.Fh

I. INTRODUCTION

Driven many-particle systems have been the topic of numerous studies in recent years [1]. The simplest example is a one-dimensional lattice gas where hard-core particles move stochastically in one direction. This model, also known as the asymmetric exclusion process, can be treated exactly, and therefore, has become a reference system in this field [2–4]. The characteristic feature of such driven systems is a nonzero current in the stationary state. For the case of open boundaries, this current transports the ''information'' from the boundaries into the bulk, and nonequilibrium phase transitions can arise [5,6]. These do not have analog in equilibrium systems where the boundaries normally do not play a significant rôle. It was shown in [7] that the phase transitions for a generic-driven system with one type of particles are governed entirely by an extremal principle for the macroscopic current $j(\rho)$, where ρ denotes the average density of the particles. This principle states that the stationary bulk current assumes its absolute minimum within the interval set by the boundary densities, if $\rho_-(\text{left}) < \rho_+(\text{right})$ and the flux is towards the right. If $\rho_- > \rho_+$ it takes its absolute maximum. In either case, the current and the density fluctuate only slightly around their stationary values and the fluctuations vanish as the system size goes to infinity.

In the present paper, we study a system with two parallel channels and show that these two properties do not hold in general. Our example is a simple extension of the one-channel model and contains one additional parameter that measures the coupling between the channels. There is no exchange of particles, but the hopping rates in one chain depend on the local configuration in the other one. They are chosen in such a way that, for a ring, the stationary state has a simple product form, and thus, the current can be obtained explicitly. With reservoirs at the ends, the system was studied by a combination of numerical and analytical methods. In a ρ_--ρ_+ phase diagram, it shows a number of regions with equal densities in both chains and various values for the current. In addition, however, there are two other regions with unexpected new features. They develop out of the first-order transition line of the single-chain problem as the interaction between the channels is turned on. In both of them, the overall densities ρ_1 and ρ_2 in the two chains fluctuate strongly and only a probability distribution $w(\rho_1,\rho_2)$ can be given. Together with that, symmetry-breaking phenomena appear.

In one region, one finds spatial coexistence between sections of equal and of unequal (but fixed) densities in the two chains, with the size of these sections varying in time. This is similar to the situation on the transition line for one chain, where sections of high and low density, separated by a domain wall, coexist. It is related to the fact that the current, which must be constant throughout the system (and thus plays the rôle of a chemical potential), can be the same for different densities. This will be called the *mixed-phase region* in the following.

In the other region, which appears if the coupling exceeds a critical value and then grows at the expense of the first one, only the unsymmetric configurations exist. The total system is then practically half filled, $\rho_1+\rho_2=1$, but the individual densities change in time. The same holds for the current. The most probable configurations are those where one channel is relatively empty and the other relatively full. Between them, the system diffuses back and forth, and hence, we will use the term *seesaw region* in the following. The time in which the channels interchange roles increases only as a power of the system size, in contrast to the result for a model with two kinds of particles on one chain [6,8] or simplified versions of it [9,10]. The situation can be compared to that at an equilibrium first-order transition with a vanishing or size-independent free-energy barrier between the phases. In this sense, the symmetry breaking could be called ''weak.'' The origin of this behavior is related to the existence of fast and slow processes in the system, as will be discussed in detail.

The paper is organized as follows. In Sec. II, we define the model and describe the solution on a ring. In Sec. III, we treat it with boundary reservoirs and present numerical results from Monte Carlo and mean-field calculations. The case of strong interactions, where one can simplify the problem and obtain analytical results for the seesaw region, is the topic of Sec. IV. After that, we turn, in Sec. V, to general interactions and establish the complete $\rho_- - \rho_+$ phase diagram. Section VI contains the conclusion and some discussion of open problems. Some details concerning the boundary rates and the mean-field equations can be found in Appendixes A and B.

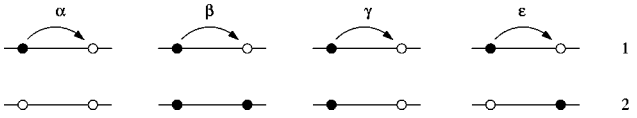

FIG. 1. The four elementary hopping processes, shown here for the first chain, and their rates. In the study, the first three rates are set equal to one.

II. MODEL

Our model consists of two parallel chains, on each of which particles can hop towards the right if the next site is empty. The hopping rate in one chain depends on the configuration of the neighboring sites in the other and one has the four processes shown in Fig. 1. The stationary state has a simple form (given below) if the rates satisfy the condition $\alpha+\beta=2\gamma$. In the following, we choose $\alpha=\beta=\gamma=1$, so that the remaining rate

$$\epsilon \equiv \exp(-\nu) \tag{1}$$

is the only parameter. It refers to those processes where the site besides the jumping particle is empty, but the next one in the forward direction is occupied. We will always assume $\epsilon<1$. This can be viewed as the result of short-range interactions that increase the barrier similar as in [11]. In a traffic-model context, ϵ would describe a hesitation to move besides another car.

The state of the system can be described either by occupation numbers n_k, m_k, or by spin variables σ_k, τ_k for the two chains. The first take the values 1(0), the latter the values $+1(-1)$ if site k is occupied (empty). For a ring with N sites, the stationary probability $P(\sigma,\tau)=P(\sigma_1,\sigma_2,\ldots,\sigma_N,\tau_1,\tau_2,\ldots,\tau_N)$ then has the Boltzmann form

$$P(\sigma,\tau)=C\prod_{k=1}^{N}\exp(-\tfrac{1}{4}\nu\sigma_k\tau_k), \tag{2}$$

which means that different sites k are uncorrelated. This can be proved by a straightforward consideration of the gain and loss processes. For the ring geometry, the stationary densities are constant and the quantities of main interest are the currents j_1, j_2 in the two chains. These can be calculated either by working in a grand canonical ensemble or via the mean-field equations of Appendix B, which are exact here due to the form of Eq. (2). For example, the mean-field expression for j_1 is, from Eq. (B1), with $p_k=n_k m_k$

$$j_1=n_k(1-n_{k+1})+(\epsilon-1)(n_k-p_k)(m_{k+1}-p_{k+1}), \tag{3}$$

where all quantities are expectation values. In the stationary state, they are independent of k, $n_k=\rho_1, m_k=\rho_2$ and one only has to determine p. The expression for the current for arbitrary densities ρ_1,ρ_2 is complicated and is omitted here. In particular cases $\rho_1=\rho_2$ or $\rho_1=1-\rho_2$, the currents in the two chains are the same and given by

$$j=\rho(1-\rho)[1\pm\{1-\sqrt{1+F(\pm\nu,\rho)}\}^2/F(\pm\nu,\rho)]; \tag{4}$$

$$F(\nu,\rho)=4(e^{-\nu}-1)\rho(1-\rho), \tag{5}$$

where the upper (lower) sign holds for $\rho_1=\rho_2=\rho$ and $\rho_1=1-\rho_2=\rho$, respectively. The resulting curves are shown in Fig. 2 for various values of the interaction parameter ν. One can see that for larger ν a minimum at $\rho=1/2$ exists in the case of equal densities. The value where this first happens is $\nu_{crit}=\ln 4\approx 1.39$. The reason is that for half filling and large ν, adjacent sites are mainly occupied by particle-hole pairs and then only hopping with the small rate ϵ is possible. Such a double-peak structure of the current leads to a much richer phase diagram in the one-chain problem with reservoirs [7] and will be important here, too.

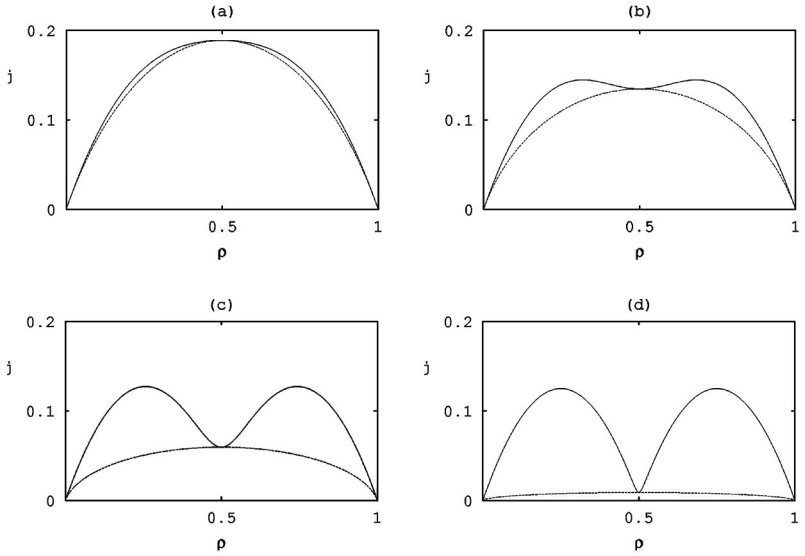

FIG. 2. Current j vs density ρ for a ring according to (3,4) for four values of the interaction, $\nu=1.2,2,4,8$ (a)–(d). Upper and lower curves correspond to $\rho=\rho_1=\rho_2$ and $\rho=\rho_1=1-\rho_2$, respectively.

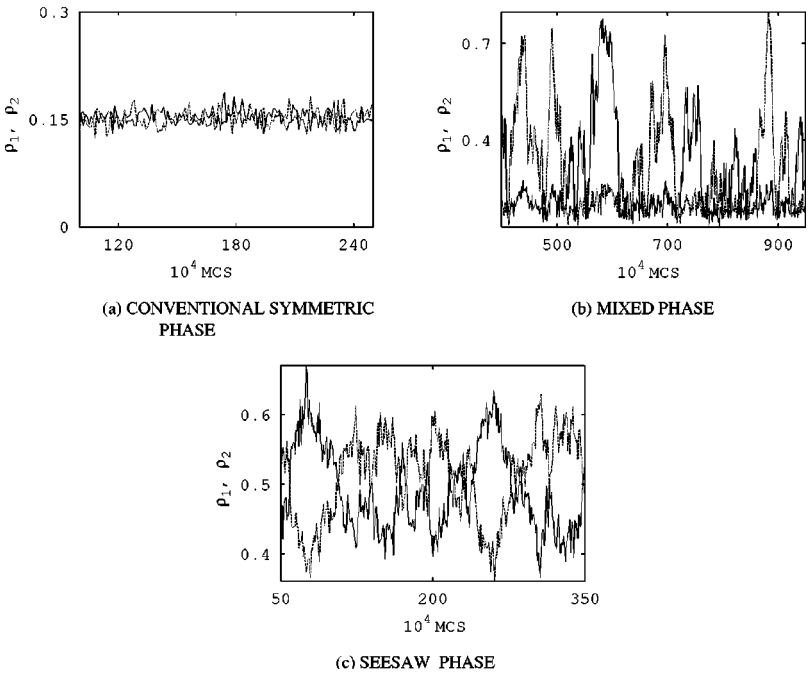

FIG. 3. Time evolution of the average densities in the two chains for three typical cases, as obtained from simulations for a system with $\nu=2$ and $N=1000$ sites. Boundary densities ρ_-,ρ_+: (a) 0.15, 0.5; (b) 0.15, 0.8; (c) 0.42, 0.6.

With reservoirs, particles enter the system at site $n=1$ and leave from site N. If one adds reservoir sites $n=0$ and $n=N+1$ to the chains, the bulk processes of Fig. 1 appear also at the boundaries. The rates can then be chosen in such a way that the dynamics is the same as in the interior, but at prescribed densities ρ_- and ρ_+ [12,7]. These are thus the only boundary parameters that enter. The procedure is described in more detail in Appendix A. In the following we will normally choose equal boundary densities for both chains, which makes the problem completely symmetric between them. Since the transport can be viewed as the motion of vacancies towards the left, it is also symmetric under the exchange $\rho_-\leftrightarrow 1-\rho_+,\rho_\alpha\leftrightarrow 1-\rho_\alpha$.

III. NUMERICS

We have performed Monte Carlo (MC) simulations of our system for different values of ρ_-,ρ_+, and ν, looking first at global quantities, namely the overall densities $\rho_1(t)$ and $\rho_2(t)$ in the two chains. The motivation for this was that, for a single chain, the average density of particles is an order parameter characterizing the different phases. This means that $\rho(t)$ fluctuates only slightly around its mean value and the fluctuations vanish as the system size grows.

Typical results of such MC calculations are presented in Fig. 3 for $\nu=2$ and three different values of the boundary densities. While in Fig. 3(a) the behavior is as for a single chain, the other two figures show a ''random walk'' of ρ_1 and ρ_2 within a large range of densities. These large fluctuations are intrinsic, they do not change qualitatively with the system size. In Fig. 3(c) the situation is still relatively simple since the sum of the densities stays approximately constant. In Fig. 3(b), however, the behavior is rather irregular and the global densities do not give a sufficient description. Rather, one has to look at the state of the system in more detail. It then turns out that the seemingly chaotic pattern is connected with the spatial coexistence of several phases.

This can already be seen in a mean-field (MF) analysis of the system. The corresponding equations are given in Appendix B. We integrated them over time, starting from random initial conditions and stopping when the current had converged to 10^{-6} in relative units. In the region of small ρ_- and large ρ_+, the mean-field density profiles then had the typical shapes seen in Fig. 4.

Let us first discuss Fig.4(a), which corresponds to $\rho_-<1-\rho_+$. Here, one has two regions where the local densities are constant. On the left they are the same in both chains, $\langle n_k\rangle,\langle m_k\rangle=\rho_-$, while on the right they are different. This leads to the bubblelike structure in the figure. That such a coexistence is possible, follows already from Fig. 2, since a given value of the current (for the ring) can be realized in different ways. Correspondingly, the densities in the bubble region are given by $\langle n_k\rangle=\hat{\rho},\langle m_k\rangle=1-\hat{\rho}$ where $j(\hat{\rho},1-\hat{\rho})=j(\rho_-,\rho_-)$. The left end of the bubble can be anywhere, its location depends on the initial conditions. Similarly, the two channels can exchange roles. However, the bubble is always ''glued'' to the right boundary. For $\rho_->1-\rho_+$, one has a similar picture but the region with equal densities now appears on the right and the values are $\langle n_k\rangle,\langle m_k\rangle=\rho_+$. This is a consequence of the particle-hole symmetry of the model. The bubble in this case is attached to the left boundary, while the location of its right end depends on the initial conditions. Finally, on the line $\rho_-=1-\rho_+$, see Fig. 4(b), the bubble coexists with *two* regions, one to the left and one to the right, where the density in both chains is the same. On the left its value is ρ_-, on the right it is ρ_+. These regions can coexist, because $j(\rho,\rho)=j(1-\rho,1-\rho)$. In this case, the locations of

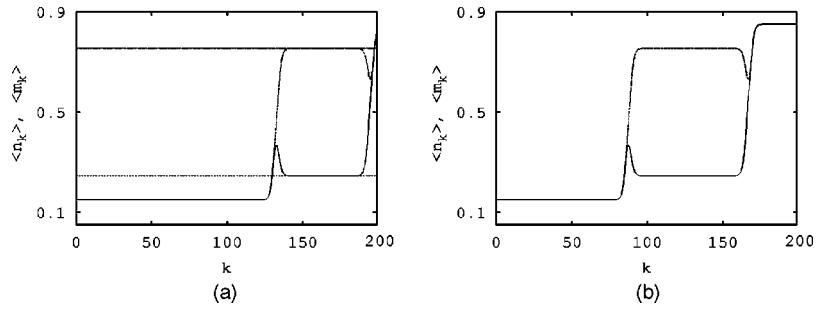

FIG. 4. Density profiles in the mean-field approximation for a system with $\nu=2$ and $N=200$ sites. Boundary densities ρ_-,ρ_+: (a) 0.15, 0.82; (b) 0.15, 0.85. The horizontal lines indicate the densities $\hat{\rho},1-\hat{\rho}$ predicted by equating the currents $j(\hat{\rho},1-\hat{\rho})=j(\rho_-,\rho_-)$, see Sec. III.

both ends of the bubble depend on the initial conditions.

In order to verify the correctness of this MF picture, we performed specific Monte Carlo simulations. In the spirit of [18,16], we introduced two phantom particles A and B designed to track down the left and right end of a bubble, respectively. Denoting the position of particle A by a, the rules are

$$a\to a+1, \quad \text{if } n_{a+1}=0,\ m_{a+1}=0, \tag{6}$$

$$a\to a-1, \quad \text{if } (1-n_{a-1})(1-m_{a-1})=0. \tag{7}$$

This means that A moves preferentially to the right in a low-density region and preferentially to the left in a high-density region, including the bubble region. In contrast to the second-class particles in Ref. [16], A does not use the sites of the chains and should rather be viewed as moving besides them. Its dynamics does not interfere with that of the chain particles. Analogously, the dynamics of particle B with coordinate b is

$$b\to b-1, \quad \text{if } n_{b-1}=1,\ m_{b-1}=1, \tag{8}$$

$$b\to b+1, \quad \text{if } n_{b-1}m_{b-1}=0, \tag{9}$$

and it therefore tracks the right end of a bubble.

One then runs the MC simulations, adds particles A and B at some point and monitors their positions. For $\rho_-<1-\rho_+$, it turns out that A performs a random walk, while B basically sticks to the right boundary, $b\approx N$. It is then interesting to look at those configurations, where A is at a certain specified site. Thereby one singles out the states with a particular size of the bubble region (if there is one). The average density profile in this case is shown in Fig. 5 for $\rho_-=0.15$, $\rho_+=0.77$. Quite remarkably, it has the same shape as found in the mean-field calculations [17]. This confirms that, indeed, there is a very unusual dynamical coexistence of various states. The MC calculations also confirm that the size of the bubble region can vary and that the two chains can interchange roles. While this is related to the initial conditions in the MF treatment, it happens dynamically here.

For the case of Fig. 3(c) the situation is different. As mentioned, the system is always half filled, i.e., $\rho_1(t)+\rho_2(t)=1$ during the evolution. For given overall densities ρ_1,ρ_2, one finds an average profile with one bubble that fills essentially the whole system. Thus, there is no spatial coexistence of different regions along the chains. However, the densities individually fluctuate strongly in an interval

$$\rho_{min}\leqslant\rho_{1,2}\leqslant\rho_{max}, \tag{10}$$

where roughly $\rho_{min}=\max(\rho_-,1-\rho_+)$, $\rho_{max}=1-\rho_{min}$. A small asymmetry h in the boundary densities (a field in magnetic language) suppresses these fluctuations. If one chooses

$$\rho_{-,1}=\rho_--h,\ \rho_{-,2}=\rho_-,\quad \rho_{+,1}=\rho_+,\quad \rho_{+,2}=\rho_++h, \tag{11}$$

which makes the chains inequivalent without destroying the particle-hole symmetry, the system locks in at $\rho_1=\rho_{min}$, $\rho_2=\rho_{max}$ or vice versa, depending on the sign of h. Moreover, if one computes formally a ''free-energy density'' $f(M)=-\ln[w(M)]/N$ at small field, where $w(M)$ is the stationary probability to have M particles in one channel, it has exactly the same form as found for a single chain in the vicinity of the line of first-order transitions, see Fig. 18 in [8]. Therefore, the whole region where this occurs (and which we will determine in more detail below) can be viewed as one of first-order transitions.

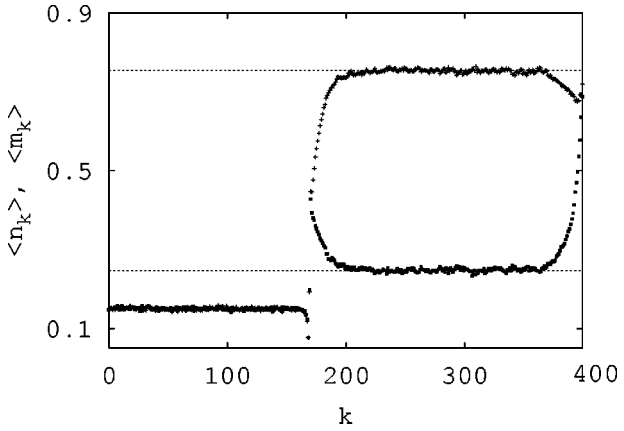

FIG. 5. Average density profiles as seen from a second-class particle positioned at site 170, provided the density in the first chain is higher, for a system with $\nu=2$, $\rho_-=0.15$, $\rho_+=0.77$, and $N=400$ sites. The average is taken over $6*10^7$ Monte Carlo steps after $3*10^5$ steps of equilibration. The horizontal lines indicate the densities $\hat{\rho},1-\hat{\rho}$ predicted by equating the currents $j(\hat{\rho},1-\hat{\rho})=j(\rho_-,\rho_-)$, see Sec. III.

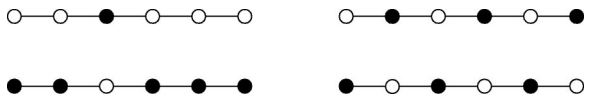

FIG. 6. Two examples of metastable states, see text.

IV. STRONG-INTERACTION LIMIT

The behavior described at the end of the previous section is found in the whole domain of reservoir densities

$$\rho_- < 1/2; \quad \rho_+ > 1/2 \tag{12}$$

if the interaction between the channels is strong, i.e., if $\nu \gg 1$ ($\epsilon \ll 1$). In this limit, the problem can be discussed analytically, as we now show.

The basic observation is that in this case *three* of the boundary processes are slow (with rate of order ϵ) and only *one* (where on the left both sites are empty or on the right both sites are full) is fast (rate of order 1). This comes from the construction of the boundary rates mentioned above and is discussed in more detail in Appendix A. As a consequence, there exist particular configurations, which can be left only with rate ϵ, and that we will call metastable. These are such that the system is half filled, with M particles in the first and $N-M$ in the second channel, arranged in such a way that adjacent sites are always in a particle-hole state. Two examples are shown in Fig. 6. Transitions between such states have the character of avalanches. After a slow process, either at the boundary or in the interior, a sequence of N fast processes follows after which a new metastable configuration is reached. If the start is in the bulk, four different final configurations with $M' = M$, $M \pm 1$ can be reached according to

$$M \to \begin{cases} M & \text{with probability} \quad 1/2 \\ M+1 & \text{with probability} \quad 1/4. \\ M-1 & \text{with probability} \quad 1/4 \end{cases} \tag{13}$$

A process in the bulk starts at a wall, where the orientation of the particle-hole pairs changes. For example, the first configuration in Fig. 6 has two such walls. For a given M, the average number of walls can be shown to be $\sim M(1 - M/N)$. Therefore, the average rate for bulk processes from level M is given by

$$\alpha_M \sim M(1 - M/N)\epsilon/4. \tag{14}$$

Similar considerations apply to the processes starting at the boundaries. Here, two final configurations $M' = M$ and $M' = M+1$ or $M' = M-1$ can be reached with equal probability. However, the rate does not involve M, and thus, these processes are unimportant compared to the bulk processes except for very small M or $N-M$. In the following, we will neglect them.

The dynamics of the metastable states is thus equivalent to a random walk in the space of occupation numbers $0 \leqslant M \leqslant N$ with a position-dependent rate given by Eq. (14). This rate, which in terms of the density $\rho_1 = \rho = M/N$ is proportional to $\rho(1-\rho)$, is small at the ends of the interval and large in the middle. Therefore, the system will spend most of its time near $M = 0$ and $M = N$. This can be made more precise by writing down the master equation for the probability w_M to find the value M

$$\frac{\partial w_M}{\partial t} = \alpha_{M+1} w_{M+1} + \alpha_{M-1} w_{M-1} - 2\alpha_M w_M . \tag{15}$$

In a continuum limit, this becomes

$$\frac{\partial w(\rho)}{\partial t} = \frac{\partial^2}{\partial \rho^2}[D(\rho) w(\rho)], \tag{16}$$

where $D(\rho) = \alpha_M / N^2$ is the diffusion constant. This equation can be related to the associated Legendre differential equation. However, for the stationary state it is sufficient to note that the probability current is given by

$$I(\rho) = -\frac{\partial}{\partial \rho}[D(\rho) w(\rho)]. \tag{17}$$

Since this has to be zero, the stationary distribution follows as

$$w(\rho) = \frac{A}{\rho(1-\rho)}; \quad 0 < \rho < 1. \tag{18}$$

This simple universal function, which is independent of the parameters of the system, is also seen in simulations as illustrated in Fig. 7(a). Actually, the picture shows some deviations at the boundaries of the interval, but there the neglected processes should be included. This would lead to finite rates also at $\rho = 0,1$ and prevent $w(\rho)$ from diverging there. In order to normalize it as it stands, one has to leave out a small boundary region of width δ/N.

Although the system is mainly in configurations with the density in one chain small and in the other large, it is not locked into them. The average time in which the two chains interchange roles can be calculated from the first passage time formula given in [13]. In the continuum case it reads

$$T = \int_{\delta/N}^{1-\delta/N} d\rho w(\rho) \int_{\delta/N}^{1/2} \frac{d\rho'}{D(\rho') w(\rho')} = N \ln(N/\delta)/\epsilon. \tag{19}$$

Thus, T is smaller than for a homogeneous diffusion process where it varies as N^2. This is due to the large hopping rates proportional to N for intermediate values of ρ. The law is also found numerically, as seen from Fig. 7(b). However, this result and the considerations so far do not apply to arbitrarily large system sizes.

If N becomes too large, the typical time $1/N\epsilon$ after which a new slow process starts, becomes smaller than the time $\tau = N$ needed to complete the first one. Therefore, the previous considerations are limited to sizes such that $N^2\epsilon \lesssim 1$. For larger systems, it is not possible to separate the fast and the slow processes. Nevertheless, the system is still basically half filled and each time a particle comes in and another particle exits, the number M changes according to Eq. (13).

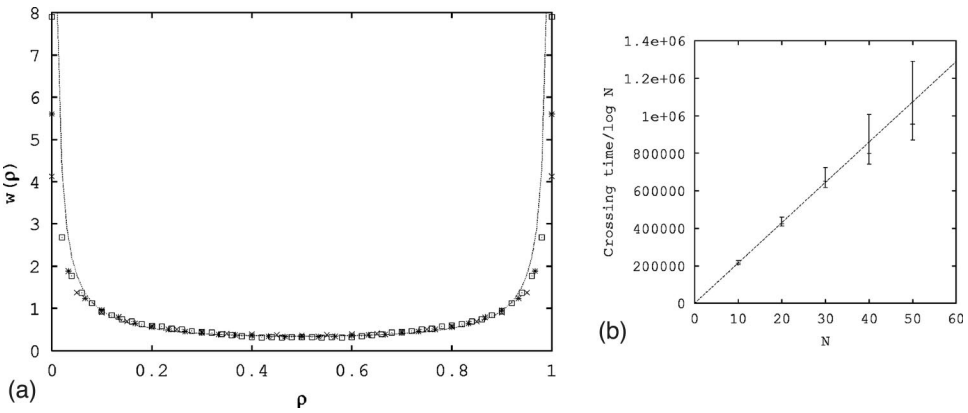

FIG. 7. (a) Stationary probability distribution $w(\rho)$ for small systems in the seesaw region. Analytical result (18) (continuous curve) in comparison with data from Monte Carlo simulations of systems with $\nu=8$, $\rho_-=0.1$, $\rho_+=0.9$, and $N=20,30,50$ sites (crosses, stars, and boxes). The systems have evolved for at least 10^7 Monte Carlo steps, the averages are taken over 40 histories. (b) The corresponding average passage times.

Since these processes also determine the flux through the system, their effective rate can be related to $j(\rho,1-\rho)$. Thus, instead of Eq. (14), one has

$$\alpha_M = j(\rho,1-\rho)/2, \tag{20}$$

where for j one can use the ring result (4). This should give the behavior in the thermodynamic limit. Following the same steps as before, one then obtains the distribution

$$w(\rho)=\frac{A}{j(\rho,1-\rho)}; \quad \rho \ \text{ within the limits(10)} \tag{21}$$

for the density ρ. This is again independent of the boundary values $\rho_\pm$, and the interaction enters only via the formula for the current. The function is qualitatively similar to Eq. (18) but, according to the form of j (cf. Fig. 2), has a flatter shape. This behavior is clearly seen in simulations. Figure 8 shows numerical results for a system of 300 sites together with the analytical prediction. Again, there are deviations in the boundary regions near $\rho=0$ and $\rho=1$ due to Eq. (10) but apart from that the agreement is very good. The curve (18), plotted for comparison, clearly does not fit the data. Note that the rate (20) does not contain the size any more. Therefore, the passage time T is now proportional to N^2. In contrast to the diffusion model treated in [9,10] there is no exponential increase with the size.

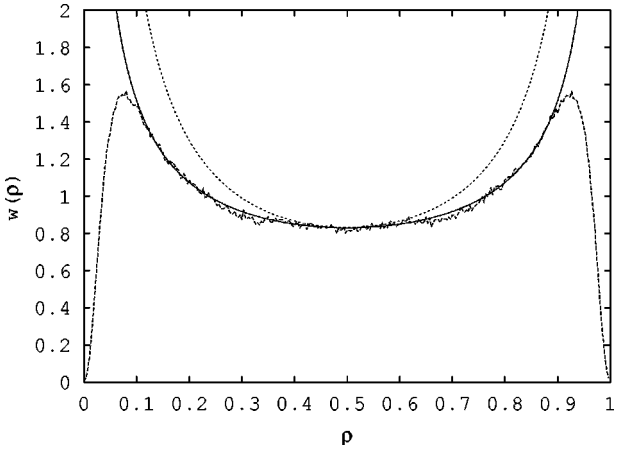

FIG. 8. Stationary probability distribution $w(\rho)$ for a large system in the seesaw phase. Analytical result (21) together with simulation data for a system of $N=300$ sites from 1.5×10^7 Monte Carlo steps, averaging over 40 histories. The parameters are $\nu=4$, $\rho_-=0.2$ and $\rho_+=0.8$. The result (18) is also shown for comparison (dotted).

V. PHASE DIAGRAM

The boundaries of the seesaw region discussed above, but also of the mixed region, depend on the interaction parameter ν and can be found from the following argument. Let us fix $\rho_+>1/2$ and gradually increase ρ_-. For very small ρ_-, it takes the time $t\approx 1/\rho_-$ to fill an empty site from the reservoir, which is longer than the time $1/\epsilon$ for slow processes to happen in the bulk. In this case the system will go into the symmetric low-density phase which also exists in the lower left corner of the $\rho_- - \rho_+$ phase diagram. As $\rho_-<\rho_+$, it will tend to minimize its flux according to the minimization principle [7] and the stationary current will be $j(\rho_-,\rho_-)$. But this principle, extended to the two-channel case, suggests that the low-density phase will become unstable if there is a region (ρ_1,ρ_2) such that the currents in both channels are smaller than $j(\rho_-,\rho_-)$

$$j_\alpha(\rho_1,\rho_2)<j(\rho_-,\rho_-); \quad \rho_-<\rho_1,\rho_2<\rho_+. \tag{22}$$

A transition will take place as soon as the first such point appears. For our system, this happens at $\rho_1=1-\rho_2=\rho_+$ and therefore the instability is expected when

$$j(\rho_-,\rho_-)=j(\rho_+,1-\rho_+), \tag{23}$$

i.e., when the upper and the lower curves in Fig. 2 lead to the same current. Actually, according to the results in Sec. III, the low-density phase does not vanish completely but coexists with unsymmetric configurations beyond that point.

The part of the region (22) along the diagonal $\rho_1+\rho_2=1$ consists of two separated segments [compare Figs.

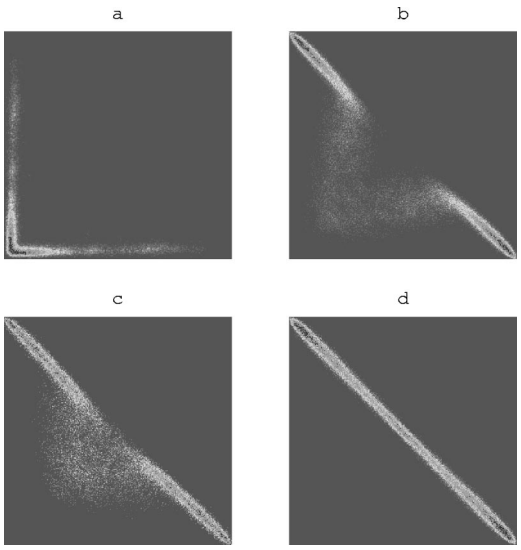

FIG. 9. Stationary distribution $w(\rho_1,\rho_2)$ as obtained from numerical simulations for a system of 300 sites with $\nu=4$, $\rho_+=0.8$, and $\rho_-=0.02,0.055,0.06,0.09$ (a–d). The figures show the location of nonzero w, the dark regions within white ones correspond to the highest values of w.

9(b,c)]. As ρ_- grows, these segments also grow until they finally merge at a value ρ^* such that

$$j(\rho^*,\rho^*)=j(1/2,1/2). \tag{24}$$

From that point onwards, the low-density symmetric region (the presence of which is signaled by the ''cloudy'' part in Figs. 9(b,c) disappears completely and the seesaw phase described in the previous section takes over. A further increase of ρ_-, however, decreases the range within which ρ_1 and ρ_2, according to Eqs. (22), (10), may fluctuate. At $\rho_-=1/2$ the system crosses the boundary into the symmetric phase with $\rho_1=\rho_2=\rho_+$ via a second-order transition [see Figs. 10(b,c)].

These simple arguments are well supported by Monte Carlo calculations. In Fig. 9, the stationary density distribution $w(\rho_1,\rho_2)$ is shown for fixed ρ_+ and four different values of ρ_-. The change of its shape as one crosses the points defined by Eqs. (23,24) is clearly seen. In Fig. 9(a), the system is in the conventional low-density phase. The distribution has a boomerang shape due to the finite size (incidentally similar to the one found in [8]) with the weight however concentrated on a symmetric line $\rho_1=\rho_2$ near the origin.

In Fig. 9(d), on the other hand, there is only weight along the diagonal $\rho_1+\rho_2=1$, which is characteristic of the seesaw region. Figures 9(b) and 9(c) show the transition region between Eqs. (23) and (24) and indicate the mixed phase. The ''cloudy'' part in Figs. 9(b) and 9(c) is due to the coexistence of symmetric and asymmetric states mentioned above and the increasing weight along the diagonal comes from an increase of density values satisfying Eq. (22). The mixed region, as seen in Figs. 10(a)–10(c), exists for all values $\epsilon<1$. By contrast, the seesaw region only appears when ϵ becomes smaller than $\epsilon_{crit}=1/4$, the value where the symmetric current $j(\rho,\rho)$ starts to develop a double-hump structure.

The discussion so far has assumed that the value of ρ_+, for which one varies ρ_-, is not too large. If $\rho_+>\rho^*$, where ρ^* is defined by Eq. (24), and one increases ρ_-, one will still cross the transition line at the point given by Eq. (23). With further increase of ρ_-, however, the condition (24) will not be satisfied, and the system will remain in the mixed region. Upon crossing the line $\rho_+=1-\rho_-$, the coexistence of symmetric it low-density regions with asymmetric ones changes into a coexistence of symmetric *high-density* regions with asymmetric ones. Finally, one ends up in the conventional high-density phase.

One should mention that if one analyzes the situation more closely with second-class particles, one finds that the fraction of symmetric and unsymmetric configurations changes as one moves through the mixed-phase region. This leads to the changing ''cloud'' mentioned above. However, we do not discuss this in more detail here.

The complete $\rho_--\rho_+$ -phase diagram is drawn in Figs. 10 (a–c) for three different values of the interaction. The sequence shows in particular how the two new regions develop in the upper-left corner as ν is increased. In the noninteracting case, the mixed region shrinks to the upper-left part of the diagonal and becomes the single-chain transition line. The remaining regions are occupied by symmetric phases with $\rho_1=\rho_2$, and the boundaries are determined by the extremal principle for the current $j(\rho,\rho)$, given by Eq. (4). This happens because outside the region (12) the evolution of the system at the boundaries is governed by the fast processes. For instance, if $\rho_->1/2$, the injection rate will be fast. This will produce a considerable number of adjacent pairs of particles in the bulk and consequently the extraction will also be due to the fast processes. For the symmetric boundary densities which we consider, a symmetric bulk situation is to be expected. But then each chain behaves es-

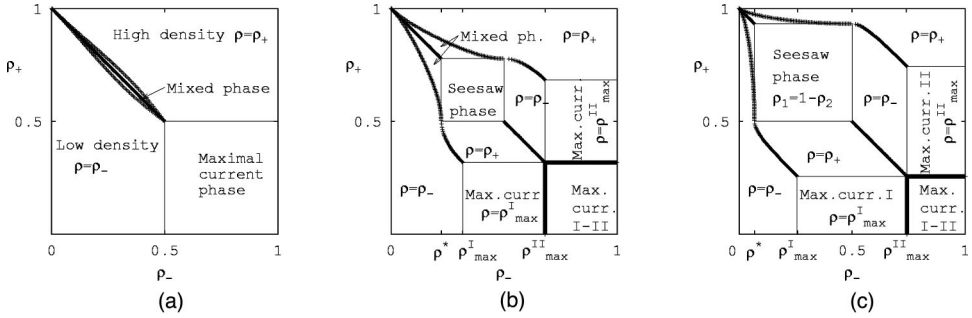

FIG. 10. Phase diagram of the model for three different values of the coupling: $(a)\,\nu=1$, $(b)\,\nu=2$, $(c)\,\nu=4$. Thick (thin) lines indicate first- (second-)order transitions. ρ^I_{max} and ρ^{II}_{max} denote the positions of the left and right maximum of the curve $j(\rho,\rho)$ in Fig. 2.

sentially like an independent one with current $j(\rho)=j(\rho,\rho)$. Consequently, the problem falls into the class considered in [7]. In drawing the boundaries, the symmetry of the problem (see the end of Sec. II) was used. They were also checked by simulations.

VI. CONCLUSION

We have studied the problem of a two-channel system, coupled to reservoirs of prescribed densities, through which a current flows. The aim was to see which phases one can expect in such a system, and what the principles are that govern the transitions between them. The example we took was a one-parameter model that has a simple stationary state on a ring. We found that already this system shows complex behavior in certain parts of the parameter space.

The mixed-phase region is probably the simpler phenomenon. A relatively close analogy in equilibrium statistical physics can be found in a system of two ferromagnetic planes that are coupled together antiferromagnetically. The coexistence line $H=0$, $T<T_c$ of the single layers in a uniform field H then widens into a whole region in the $T-H$ plane, and if one creates domain walls by identical boundary conditions on both layers, these tend to separate in space, creating bubble regions of opposite magnetizations, while a nonzero field favors regions of equal magnetizations. Thus, one finds features as in Figs. 4 and 5.

The seesaw region with its ''weak'' symmetry breaking is more interesting, and we studied it in more detail. One might view the phenomenon as a kind of phase-separation *between* the channels, as opposed to the one *along* the channels in the mixed-phase region. There are also certain similarities to critical phases. On the one hand, the probability distribution $w(\rho)$ resembles that for the order parameter of a finite Ising system at the critical temperature [14]. One the other hand, its properties do not depend (except for the left and right limits) on the boundary values $\rho_\pm$, a feature that it shares with the critical (maximal-current) phase found in the present model.

One should note that our model differs from the lattice-gas models studied in [15,1], since the particles cannot hop between the chains. It would be interesting to see whether relaxing these conservation laws changes the situation strongly. Leaving this aspect aside, however, it seems that the results are rather general. We did use the microscopic details for arguing in the paper, but the final results do not depend on them directly. It is only the flux, which determines the phase transition lines and characterizes the new phases. Thus, one can hope that pursuing this approach would allow to formulate generic principles that govern the phase transitions in such multichannel systems.

ACKNOWLEDGEMENTS

We have benefited from discussions with W. Dieterich, G. Schütz, and in particular, V. Rittenberg. V.P. would like to thank the Alexander von Humboldt Foundation for financial support.

APPENDIX A: BOUNDARY RATES

In our model, we view the reservoirs as extensions of the system having the same properties as the ring [12]. This permits a natural definition of the boundary rates. Consider, for example, the first process in Fig. 1. On the ring, it leads to the average current

$$\langle j_l\rangle=\alpha\langle n_l(1-m_l)\rangle\langle n_{l+1}(1-m_{l+1})\rangle \tag{A1}$$

between sites l and $l+1$. Here, the product form of the stationary state has been used. If site l belongs to the left reservoir, one combines α with the first factor, evaluated for the prescribed boundary densities $\rho_1=\rho_2=\rho_-$. This gives the rate

$$\alpha_-=\alpha\langle n(1-m)\rangle\rho_-. \tag{A2}$$

Analogously, if site $(l+1)$ belongs to the right reservoir, one combines α with the second factor and defines

$$\alpha_+=\alpha\langle(1-n)(1-m)\rangle\rho_+. \tag{A3}$$

In this way, one obtains boundary rates that are determined by the bulk ones, multiplied by the weight of the boundary configuration involved in the process. With $\alpha=\beta=\gamma=1$, one has

$$\alpha_-=\rho_--p_-;\quad \beta_-=\gamma_-=p_-;\quad \epsilon_-=\epsilon(\rho_--p_-); \tag{A4}$$

$$\alpha_+=\gamma_+=p_++1-2\rho_+;\quad \beta_+=\rho_+-p_+;$$

$$\epsilon_+=\epsilon(\rho_+-p_+), \tag{A5}$$

where $p_\pm=p(\rho_\pm)=\langle nm\rangle\rho_\pm$ and $p(\rho)$ is given by

$$p(\rho)=\rho+[\sqrt{(2\rho-1)^2-4\epsilon\rho(1-\rho)}-1]/2(1-\epsilon). \tag{A6}$$

For $\epsilon\ll 1$, configurations with two particles (holes) at one site have a small weight if $\rho<1/2$ $(\rho>1/2)$. Thus, for $\rho_-<1/2$ and $\rho_+>1/2$, the rates $\beta_-,\gamma_-,\alpha_+,\gamma_+$ are proportional to ϵ, as are the rates $\epsilon_\pm$. In this case, only one fast boundary process remains at each end.

With these quantities, one can then write down the total rates for the boundary processes. For example, if the first sites of both chains are empty, the rate with which a particle enters one chain is given by $(\alpha_-+\gamma_-)$. As a consequence, the currents at the left and the right end of the first chain are, respectively,

$$j_-^1=(\alpha_-+\gamma_-)(1-n_1)(1-m_1)+(\beta_-+\epsilon_-)(1-n_1)m_1; \tag{A7}$$

$$j_+^1=(\beta_++\gamma_+)n_Nm_N+(\alpha_++\epsilon_+)n_N(1-m_N). \tag{A8}$$

If $\rho_-=\rho_+$, the stationary state of the system is automatically the same as for the ring, i.e., the density is constant everywhere. This is the basic motivation for the approach described here. For $\epsilon=1$ everything reduces to the single-chain problem [2,3].

APPENDIX B: MEAN-FIELD EQUATIONS

In the mean-field approximation, one neglects the correlations between different sites. In our case, the system on a *ring* has no correlations in the stationary state $\langle n_l n_k \rangle = \langle n_l \rangle \times \langle n_k \rangle$. Two adjacent sites on different chains, however, are correlated. Therefore one should take the product $p_l = n_l m_l$ as an independent variable. Keeping this in mind, the mean-field equations resulting from the gain and the loss processes become (for $\alpha = \beta = \gamma = 1$ and leaving out the averaging brackets for simplicity)

$$\frac{\partial n_k}{\partial t} = j_k^1 - j_{k+1}^1 = [n_{k-1}(1-n_k) + (\epsilon - 1)(n_{k-1} - p_{k-1}) \times (m_k - p_k)] - [n_k(1-n_{k+1}) + (\epsilon - 1)(n_k - p_k) \times (m_{k+1} - p_{k+1})], \tag{B1}$$

$$\frac{\partial p_k}{\partial t} = (n_k - p_k)(\epsilon m_{k-1} + (1-\epsilon)p_{k-1}) + (m_k - p_k) \times (\epsilon n_{k-1} + (1-\epsilon)p_{k-1}) - p_k(2 - n_{k+1} - m_{k+1}). \tag{B2}$$

The equation for the m_k is obtained by substituting $m \leftrightarrow n$ in Eq. (B1).

The homogeneous solution of these equations $m_k \equiv m$, $n_k \equiv n$, $p_k \equiv p$ leads to a quadratic equation for p. When substituted into the expression for the current in Eq. (B1), this reproduces the value (4) because the mean-field equations are exact in this case.

For the open system, Eqs. (B1) and (B2) should be supplemented by the boundary conditions $n_0 = m_0 = \rho_-$, $n_{N+1} = m_{N+1} = \rho_+$. For p_k one takes the homogeneous solution at both ends.

[1] For a review, see, Vol. 17 B. Schmittmann and R. K. P. Zia, in *Phase Transitions and Critical Phenomena*, edited by C. Domb and J. Lebowitz (Academic, New York, 1995), Vol. 17; G. M. Schütz, in *Phase Transitions and Critical Phenomena*, edited by C. Domb and J. Lebowitz (Academic, London, 2000), Vol. 19.

[2] G. Schütz and E. Domany, J. Stat. Phys. **72**, 277 (1993).

[3] B. Derrida, M. R. Evans, V. Hakim, and V. Pasquier, J. Phys. A **26**, 1493 (1993); B. Derrida and J. L. Lebowitz, Phys. Rev. Lett. **80**, 209 (1998).

[4] F. Rezakhanlou, Commun. Math. Phys. **140**, 417 (1991).

[5] J. Krug, Phys. Rev. Lett. **67**, 1882 (1991).

[6] M. R. Evans, D. P. Foster, C. Godrèche, and D. Mukamel, Phys. Rev. Lett. **74**, 208 (1995); J. Stat. Phys. **80**, 69 (1995).

[7] V. Popkov and G. M. Schütz, Europhys. Lett. **48**, 257 (1999).

[8] P. F. Arndt, T. Heinzel, and V. Rittenberg, J. Stat. Phys. **90**, 783 (1998).

[9] C. Godrèche, J. M. Luck, M. R. Evans, D. Mukamel, S. Sandow, and E. R. Speer, J. Phys. A **28**, 6039 (1995).

[10] P. F. Arndt and T. Heinzel, J. Stat. Phys. **92**, 837 (1998).

[11] H. Singer and I. Peschel, Z. Phys. B **39**, 333 (1980).

[12] T. Antal and G. M. Schütz, Phys. Rev. E **62**, 83 (2000).

[13] N. G. van Kampen, *Stochastic Processes in Physics and Chemistry* (North-Holland, Amsterdam, 1981), Chap. 11, Eq. (2.15).

[14] K. Binder, *Finite-Size Effects at Phase Transitions*, in *Computational Methods in Field Theory*, edited by H. Gausterer and C. B. Lang, Lecture Notes in Physics, Vol. 409 (Springer, New York, 1992).

[15] S. Katz, J. Lebowitz, and H. Spohn, J. Stat. Phys. **34**, 497 (1994).

[16] B. Derrida, S. A. Janowsky, J. L. Lebowitz, and E. R. Speer, J. Stat. Phys. **73**, 813 (1993).

[17] The local decrease of the average density at the left end of the bubble is an artifact of the chosen rates. Particle *A* tends to have empty sites in both chains immediately to its left.

[18] P. Ferrari, C. Kipnis, and E. Saada, Ann. Prob. **19**, 226 (1991).